VNU Journal of Science: Mathematics – Physics, Vol. 39, No. 4 (2023) 26-43

VNU Journal of Science: Mathematics - Physics

Journal homepage: https://js.vnu.edu.vn/MaP

Original Article

Static Buckling and Free Vibration Analysis of Aligned CNTs Reinforced Composite Plates

Pham Dinh Nguyen*, Do Thi Thu Ha, Duong Tuan Manh

VNU University of Engineering and Technology, 144 Xuan Thuy, Cau Giay, Hanoi, Vietnam

Received 14 September 2023
Revised 03 October 2023; Accepted 15 October 2023

Abstract*:* This work introduces an analysis of the nonlinear buckling and free vibration behavior of polymer plates reinforced with aligned carbon nanotubes using Reddy's third-order shear deformation plate theory and incorporating Theodore von Kármán's geometric nonlinearity. The polymer plates were enhanced with single-walled carbon nanotubes assumed to exhibit either uniform distribution or functionally graded distribution across the thickness. The equations of motion were established through Hamilton’s principle and then solved by the Galerkin method and Airy’s stress function for the composite plates with fully simply supported edges. The investigation focused on assessing the effects of carbon nanotube distribution, volume fraction, and geometrical parameters on the buckling load and fundamental frequency parameters of composite plates through numerical results.

Keywords: Analytical Approach, Free Vibration, Aligned carbon nanotubes, Composite plates, Static Buckling.

1. Introduction

The unique mechanical characteristics of carbon nanotubes (CNTs) enable them to effectively serve as reinforcement components, enhancing the properties of metals, ceramics, and polymers. The incorporation of CNTs into these materials enhances composite strength, stiffness, toughness, wear resistance, electrical conductivity, thermal conductivity, and heat dissipation. As a result, CNTs reinforced composites find application across a broad spectrum of industries, including aerospace, automotive, energy, and mechanical engineering [1-4]. The concept of functionally graded distribution

* Corresponding author.
Email address: nguyenpd@vnu.edu.vn

https//doi.org/ 10.25073/2588-1124/vnumap.4876

of CNTs (FG-CNTs) reinforced composites using molecular dynamics and the rule of mixture for nonlinear bending analysis was initially introduced in a pioneering study by Shen [5]. Subsequently, Shen and Zhu [6] extended this research to include an analysis of the buckling and post-buckling behavior of plates under thermal conditions. Furthermore, various researchers have extensively employed the Halpin-Tsai model [7, 8] to investigate the mechanical properties of FG-CNTs reinforced composites. In addition, the Mori-Tanaka model has been utilized by different research groups [9, 10] to study these composites.

Buckling analysis holds significant importance in structural engineering, and numerous studies have addressed the topic of CNTs reinforced composite plates. These studies typically employ the finite element method or the analytical method. The authors in [11-20] present an investigation of the buckling behavior of composite plates reinforced with CNTs using the first-order shear deformation plate (FSDT) and finite element approach. Zhang et al., [11, 12] presented the buckling load and load-deflection curve of composite thick skew plates with uniaxially aligned CNTs and graded material properties, utilizing the element-free IMLS-Ritz method. Torabi et al., [13] formulated a unified numerical approach using the variational differential quadrature method (DQM) in conjunction with a coordinate transformation procedure for investigating the linear thermal buckling behavior in composite plates of different shapes, which are reinforced with FG-CNTs. Peng et al., [14] presented the buckling behavior of thin rectangular composite plates reinforced by CNTs under arbitrarily distributed partial edge compression, utilizing DQM and the work equivalent method to determine the pre-buckling stress distribution. Civaleka and Jalaei [15] utilized the geometric mapping discrete singular convolution method to analyze shear buckling in skew plates composed of FG composites and FG-CNTRC, involving the utilization of two distinct singular kernels along with the discretization of the singular convolution procedure. Kiani and Mirzaei [16-19] conducted an investigation into the thermal buckling, thermal post-buckling, and shear buckling behavior of rectangular plates reinforced with CNTs employing a two-dimensional Ritz formulation with Chebyshev basis polynomials to determine the elastic and geometric stiffness matrices for these plates. Hussain [20] introduced a suitable finite element model for SWCNTs reinforced composite plate, which was developed using ANSYS parametric design language code in the ANSYS environment to obtain the buckling load.

Free vibration and dynamic analysis play an important role in advancing structural engineering, as it offers valuable insights, enhances safety, and drives innovation across various engineering systems, including buildings, bridges, and aerospace structures. This evaluation is critical to ensure that structures can withstand environmental factors such as earthquakes, wind, and machinery-induced vibrations. An isogeometric analysis and the higher-order shear deformation theory are employed to investigate the static and dynamic behavior of FG-CNTs reinforced composite plates by Phung Van et al., [21] and free vibration by Singh and Bhar [22]. García-Macías et al., [23] presented the results of buckling load and fundamental frequency of FG-CNT reinforced skew plates. Lei et al., [24] investigated a free vibration analysis of composite plates with arbitrary boundary conditions using the element-free kp-Ritz method. The effective material properties of CNTs reinforced composites can be estimated by either the Eshelby–Mori-Tanaka approach or the extended rule of mixture. Zhang et al., [25, 26] have provided dependable numerical solutions for the free vibration analysis of FG-CNTs reinforced composite plates with elastic edge constraints. These solutions were achieved using the element-less IMLS-Ritz method in conjunction with FSDT. Fantuzzi et al., [27] conducted the dynamic analysis of CNT reinforced composite plates with arbitrary domains and discontinuities. García-Macías et al., [28, 29] emphasized the use of metamodel-based techniques such as Kriging and RS-HDMR in conjunction with Monte Carlo Simulation for stochastic analysis. Karamanli and Aydogdu [30] reported that the dimensionless frequency differences between the two-directional FG-CNTs and the unidirectional CNT distributions are approximately 43.5% and 39% for UD and V CNT reinforced CFFF plates, and approximately 42% for the X-CNT distribution.

Utilizing the third-order shear deformation theory is crucial for accurately representing the bending, buckling, and vibration behavior of composite plates. The aim of this work is to present a semi-analytical approach that combines the third-order shear deformation theory with von Kármán's geometric nonlinearity for fully simply supported composite plates reinforced by aligned CNTs resting on an elastic foundation. The equations of motion are derived using Hamilton’s principle and subsequently solved through the Galerkin method and Airy’s stress function to determine the nonlinear buckling load and fundamental frequency of composite plates reinforced by aligned CNTs.

2. CNTs Reinforced Composites

The material properties of the plates reinforced by aligned CNTs are shown as follows:

$$E_{11} = E_{11}^{CNT} V_{CNT} \eta_1 + E_m V_m,\ E_{22} = \frac{E_{22}^{CNT} E_m \eta_2}{E_m V_{CNT} + E_{22}^{CNT} V_m},\ G_{12} = \frac{G_{12}^{CNT} G_m \eta_3}{G_m V_{CNT} + G_{12}^{CNT} V_m} \quad (1)$$

where, V_{CNT} and V_m are the volume fractions of CNTs and the polymer matrix, respectively. The parameters $\eta_i\ (i = \overline{1,3})$ are shown in Table 1 [5, 6] for CNTs embedded in Poly(methyl methacrylate) (PMMA) matrix and Poly[(m-phenylenevinylene)-co-(2,5-dioctoxy-p-phenylenevinylene)] (PmPV) matrix.

Table 1. Efficiency parameters for CNT reinforced composite plates

	V_{CNT}^*	η_1	η_2	η_3
PMMA matrix	0.12	0.137	1.022	0.715
	0.17	0.142	1.626	1.138
	0.28	0.141	1.585	1.110
PmPV matrix	0.11	0.149	0.934	0.654
	0.14	0.150	0.941	0.659
	0.17	0.149	1.381	0.967

Poisson’s ratio is determined by:

$$\upsilon_{12} = V_{CNT}^* \upsilon_{12}^{CNT} + V_m \upsilon_m, \quad (2)$$

where, υ_{12}^{CNT} and υ_m represent Poisson’s ratios of CNTs and matrix, respectively. $V_{CNT}^* = \frac{w_{CNT}}{w_{CNT} + (\rho_{CNT}/\rho_m) - (\rho_{CNT}/\rho_m) w_{CNT}}$, with w_{CNT} denotes CNT’s mass fraction, while ρ_{CNT} and ρ_m stand for the density of CNTs and matrix, respectively.

The effective density of composite plates reinforced by CNTs can be calculated as:

The calculation for the density of composite plates reinforced by CNTs can be expressed as follows:

$$\rho = \rho_{CNT} V_{CNT} + \rho_m V_m \quad (3)$$

Considering three different distributions of aligned CNTs: a uniform distribution (UD) and two functionally graded distributions of CNTs, denoted as FG-X and FG-O. In FG-X, the maximum volume fraction is located at the upper external surfaces of the plate. In FG-O, the maximum volume fraction is positioned at the midheight of the plates, as shown in Figure. 1.

(a) UD: $V_{CNT} = V_{CNT}^{*}$, (b) FG-X: $V_{CNT} = 4V_{CNT}^{*}\dfrac{|z|}{h}$, (c) FG-O: $V_{CNT} = 2V_{CNT}^{*}\left(1-2\dfrac{|z|}{h}\right)$ (4)

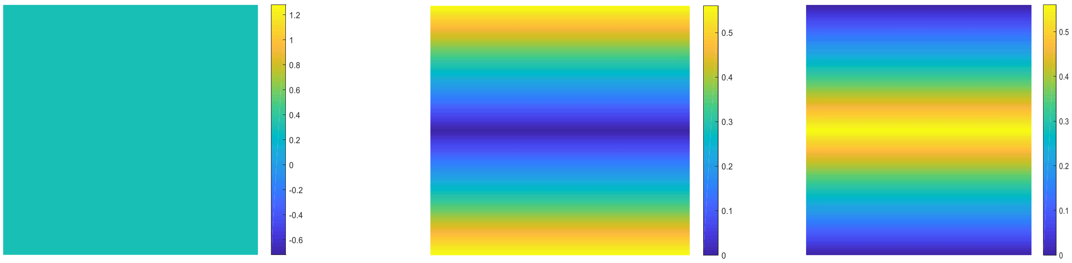

a. UD b. FG-X c. FG-O

Figure 1. Three types of CNT volume fraction of plates.

3. Formulation of Composite Plates

Consider a composite plate with following dimensions: length *a*, width*b*, and total thickness*h*. A coordinate system (x, y, z) is established, where (x, y) plane corresponds to the plate's middle surface. The z direction represents the thickness ranging from $-h/2$ to $h/2$, as illustrated in Figure 1.

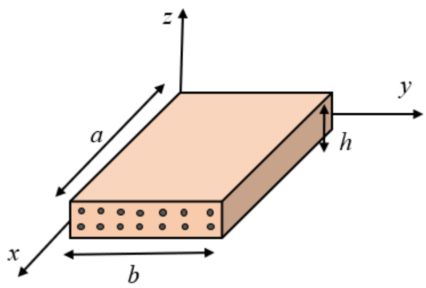

Figure 2. Model of CNTs reinforced plates.

The displacement-strain relationship, which considers Kármán's geometric nonlinearity for plates, is defined by [31]:

$$\begin{pmatrix} \varepsilon_x \\ \varepsilon_y \\ \gamma_{xy} \end{pmatrix} = \begin{pmatrix} \dfrac{\partial u}{\partial x} + \dfrac{1}{2}\left(\dfrac{\partial w}{\partial x}\right)^2 \\ \dfrac{\partial v}{\partial y} + \dfrac{1}{2}\left(\dfrac{\partial w}{\partial y}\right)^2 \\ \dfrac{\partial u}{\partial y} + \dfrac{\partial v}{\partial x} + \dfrac{\partial w}{\partial x}\dfrac{\partial w}{\partial y} \end{pmatrix}, \begin{pmatrix} \gamma_{xz} \\ \gamma_{yz} \end{pmatrix} = \begin{pmatrix} \dfrac{\partial u}{\partial z} + \dfrac{\partial w}{\partial x} \\ \dfrac{\partial v}{\partial z} + \dfrac{\partial w}{\partial y} \end{pmatrix} \quad (5)$$

The strain fields of the plate, according to Reddy's third-order shear deformation plate theory, can be expressed as follows [31]:

$$\varepsilon = \varepsilon^0 + z\varepsilon^1 + z^3\varepsilon^3,\ \gamma = \gamma^0 + z^2\gamma^2 \tag{6a}$$

where,

$$\varepsilon^0 = \begin{pmatrix} \varepsilon_x^0 \\ \varepsilon_y^0 \\ \gamma_{xy}^0 \end{pmatrix} = \begin{pmatrix} \frac{\partial u_0}{\partial x} + \frac{1}{2}\left(\frac{\partial w_0}{\partial x}\right)^2 \\ \frac{\partial v_0}{\partial y} + \frac{1}{2}\left(\frac{\partial w_0}{\partial y}\right)^2 \\ \frac{\partial u_0}{\partial y} + \frac{\partial v_0}{\partial x} + \frac{\partial w_0}{\partial x}\frac{\partial w_0}{\partial y} \end{pmatrix}, \varepsilon^1 = \begin{pmatrix} \varepsilon_x^1 \\ \varepsilon_y^1 \\ \varepsilon_{xy}^1 \end{pmatrix} = \begin{pmatrix} \frac{\partial \phi_x}{\partial x} \\ \frac{\partial \phi_y}{\partial y} \\ \frac{\partial \phi_x}{\partial y} + \frac{\partial \phi_y}{\partial x} \end{pmatrix}, \gamma^0 = \begin{pmatrix} \gamma_{xz}^0 \\ \gamma_{yz}^0 \end{pmatrix} = \begin{pmatrix} \phi_x + \frac{\partial w_0}{\partial x} \\ \phi_y + \frac{\partial w_0}{\partial y} \end{pmatrix}$$

$$\varepsilon^3 = \begin{pmatrix} \varepsilon_x^3 \\ \varepsilon_y^3 \\ \varepsilon_{xy}^3 \end{pmatrix} = -c_1 \begin{pmatrix} \frac{\partial \phi_x}{\partial x} + \frac{\partial^2 w_0}{\partial x^2} \\ \frac{\partial \phi_y}{\partial y} + \frac{\partial^2 w_0}{\partial y^2} \\ \frac{\partial \phi_x}{\partial y} + \frac{\partial \phi_y}{\partial x} + 2\frac{\partial^2 w_0}{\partial x \partial y} \end{pmatrix}, \gamma^2 = \begin{pmatrix} \gamma_{xz}^2 \\ \gamma_{yz}^2 \end{pmatrix} = -c_2 \begin{pmatrix} \phi_x + \frac{\partial w_0}{\partial x} \\ \phi_y + \frac{\partial w_0}{\partial y} \end{pmatrix}, c_1 = 4/3h^2, c_2 = 3c_1 \tag{6b}$$

The constitutive relations of the plate can be written as

$$\begin{Bmatrix} \sigma_x \\ \sigma_y \\ \sigma_{xy} \\ \sigma_{yz} \\ \sigma_{xz} \end{Bmatrix} = \begin{vmatrix} Q_{11} & Q_{12} & 0 & 0 & 0 \\ Q_{12} & Q_{22} & 0 & 0 & 0 \\ 0 & 0 & Q_{66} & 0 & 0 \\ 0 & 0 & 0 & Q_{44} & 0 \\ 0 & 0 & 0 & 0 & Q_{55} \end{vmatrix} \begin{Bmatrix} \varepsilon_x \\ \varepsilon_y \\ \gamma_{xy} \\ \gamma_{yz} \\ \gamma_{xz} \end{Bmatrix}, \tag{7a}$$

where,

$$Q_{11} = \frac{E_{11}}{1 - v_{12}v_{21}},\ Q_{12} = \frac{v_{12}E_{22}}{1 - v_{12}v_{21}},\ Q_{22} = \frac{E_{22}}{1 - v_{12}v_{21}}, Q_{44} = Q_{55} = Q_{66} = G_{12}. \tag{7b}$$

Hamilton’s principle can be stated in analytical form as:

$$\int_0^T \left(\delta U + \delta V - \delta K\right) dt = 0 \tag{8}$$

The virtual strain energy is expressed as follows:

$$\delta U = \int_A \int_{-\frac{h}{2}}^{\frac{h}{2}} \left(\sigma_x \delta\varepsilon_x + \sigma_y \delta\varepsilon_y + \sigma_{xy}\delta\gamma_{xy} + \sigma_{xz}\delta\gamma_{xz} + \sigma_{yz}\delta\gamma_{yz}\right) dz dA \tag{9}$$

The virtual work done by applied forces is determined by:

$$\delta V = \int_A \left(q_e \delta w_0\right) dA \tag{10}$$

The variation of kinetic energy due to virtual velocities is shown as:

$$\delta K = \int_A \int_{-\frac{h}{2}}^{\frac{h}{2}} \rho_z \left(\dot{u}\delta\dot{u} + \dot{v}\delta\dot{v} + \dot{w}\delta\dot{w} \right) dz dA \tag{11}$$

By substituting equations (6) and (7) into equations (9) through (11), then applying Hamilton's principle and integrating by parts, we obtain the Euler-Lagrange equations for composite plates resting on an elastic foundation as follows [31]:

$$\frac{\partial N_x}{\partial x} + \frac{\partial N_{xy}}{\partial y} = I_0 \frac{\partial^2 u_0}{\partial t^2} + J_1 \frac{\partial^2 \phi_x}{\partial t^2} - c_1 I_3 \frac{\partial^3 w_0}{\partial x \partial t^2}, \tag{12a}$$

$$\frac{\partial N_{xy}}{\partial x} + \frac{\partial N_y}{\partial y} = I_0 \frac{\partial^2 v_0}{\partial t^2} + J_1 \frac{\partial^2 \phi_y}{\partial t^2} - c_1 I_3 \frac{\partial^3 w_0}{\partial y \partial t^2}, \tag{12b}$$

$$\begin{aligned} &\frac{\partial Q_x}{\partial x} + \frac{\partial Q_y}{\partial y} - c_2 \left(\frac{\partial R_x}{\partial x} + \frac{\partial R_y}{\partial y} \right) + \frac{\partial^2 f}{\partial y^2} \left(\frac{\partial^2 w_0}{\partial x^2} \right) - 2 \frac{\partial^2 f}{\partial x \partial y} \left(\frac{\partial^2 w_0}{\partial x \partial y} \right) \\ &+ \frac{\partial^2 f}{\partial x^2} \left(\frac{\partial^2 w_0}{\partial y^2} \right) + c_1 \left(\frac{\partial^2 P_x}{\partial x^2} + 2 \frac{\partial^2 P_{xy}}{\partial x \partial y} + \frac{\partial^2 P_y}{\partial y^2} \right) - K_{\mathrm{w}} w_0 + K_P \left(\frac{\partial^2 w_0}{\partial x^2} + \frac{\partial^2 w_0}{\partial y^2} \right) \\ &= I_0 \frac{\partial^2 w_0}{\partial t^2} - c_1^2 I_6 \left(\frac{\partial^4 w_0}{\partial x^2 \partial t^2} + \frac{\partial^4 w_0}{\partial y^2 \partial t^2} \right) \\ &+ c_1 \left[\left(J_4 - \frac{J_1 I_3}{I_0} \right) \frac{\partial^3 \phi_x}{\partial x \partial t^2} + \left(J_4 - \frac{J_1 I_3}{I_0} \right) \frac{\partial^3 \phi_x}{\partial y \partial t^2} + \frac{c_1 I_3^2}{I_0} \frac{\partial^2}{\partial t^2} \left(\frac{\partial^4 w_0}{\partial x^2} + \frac{\partial^4 w_0}{\partial y^2} \right) \right] \end{aligned} \tag{12c}$$

$$\begin{aligned} &\frac{\partial M_x}{\partial x} + \frac{\partial M_{xy}}{\partial y} - c_1 \left(\frac{\partial P_x}{\partial x} + \frac{\partial P_{xy}}{\partial y} \right) - Q_x + c_2 R_x = J_1 \frac{\partial^2 u_0}{\partial t^2} \\ &+ K_2 \frac{\partial^2 \phi_x}{\partial t^2} + \left(\frac{c_1 I_3 J_1}{I_0} - c_1 J_4 \right) \frac{\partial^3 w_0}{\partial x \partial t^2} \end{aligned} \tag{12d}$$

$$\begin{aligned} &\frac{\partial M_{xy}}{\partial x} + \frac{\partial M_y}{\partial y} - c_1 \left(\frac{\partial P_{xy}}{\partial x} + \frac{\partial P_y}{\partial y} \right) - Q_y + c_2 R_y = J_1 \frac{\partial^2 v_0}{\partial t^2} \\ &+ K_2 \frac{\partial^2 \phi_y}{\partial t^2} + \left(\frac{c_1 I_3 J_1}{I_0} - c_1 J_4 \right) \frac{\partial^3 w_0}{\partial y \partial t^2} \end{aligned} \tag{12e}$$

with:

$$I_i = \int_{-\frac{h}{2}}^{\frac{h}{2}} \rho z^i dz, J_i = I_i - c_1 I_{i+2}, K_2 = I_2 - 2c_1 I_4 + c_1^2 I_6, \left(i = 0 \, \text{to} \, 6 \right) \tag{13}$$

The force resultants in terms of Airy's stress function $f\left(x, y, t\right)$ as:

$$N_x = \frac{\partial^2 f}{\partial y^2}, N_y = \frac{\partial^2 f}{\partial x^2}, N_{xy} = -\frac{\partial^2 f}{\partial x \partial y} \tag{14}$$

The geometrical compatibility equation for the plates is defined as:

$$\frac{\partial^2 \varepsilon_x^0}{\partial y^2} + \frac{\partial^2 \varepsilon_y^0}{\partial x^2} - \frac{\partial^2 \gamma_{xy}^0}{\partial x \partial y} = \left(\frac{\partial^2 w_0}{\partial x \partial y}\right)^2 - \frac{\partial^2 w_0}{\partial x^2}\frac{\partial^2 w_0}{\partial y^2} \tag{15}$$

Substituting the strain components from Eq. (7) and the stress function into Eq. (15) to obtain:

$$\begin{aligned} & A_{11}^* \frac{\partial^4 f}{\partial x^4} + A_{22}^* \frac{\partial^4 f}{\partial y^4} + \left(A_{66}^* - 2A_{12}^*\right)\frac{\partial^4 f}{\partial x^2 \partial y^2} + \left(D_{21}^* c_1 - D_{66}^* c_1 - B_{21}^* + B_{66}^*\right)\frac{\partial^3 \phi_x}{\partial x \partial y^2} \\ & + \left(B_{11}^* - D_{11}^* c_1\right)\frac{\partial^3 \phi_x}{\partial x^3} - \left(D_{12}^* c_1 + D_{66}^* c_1 - B_{12}^* - B_{66}^*\right)\frac{\partial^3 \phi_y}{\partial x^2 \partial y} + \left(D_{22}^* c_1 - B_{22}^*\right)\frac{\partial^3 \phi_y}{\partial y^3} \\ & - D_{11}^* c_1 \frac{\partial^4 w_0}{\partial x^4} + D_{22}^* c_1 \frac{\partial^4 w_0}{\partial y^4} + \left(D_{12}^* c_1 - D_{12}^* c_1 - 2D_{66}^* c_1\right)\frac{\partial^4 w_0}{\partial x^2 \partial y^2} = \left(\frac{\partial^2 w_0}{\partial x \partial y}\right)^2 - \frac{\partial^2 w_0}{\partial x^2}\frac{\partial^2 w_0}{\partial y^2} \end{aligned} \tag{16}$$

By substitution Eq. (14) into Eqs. (12) results in:

$$\begin{aligned} & X_{11}\left(w_0\right) + X_{12}\left(\phi_x\right) + X_{13}\left(\phi_y\right) + X_{14}(f) + X_{15}\left(w_0, f\right) = I_0 \frac{\partial^2 w_0}{\partial t^2} + \overline{j_1^1}\frac{\partial^4 w_0}{\partial x^2 \partial t^2} \\ & + \overline{j_1^2}\frac{\partial^4 w_0}{\partial y^2 \partial t^2} + \overline{j_1^3}\frac{\partial^3 \phi_x}{\partial x \partial t^2} + \overline{j_1^4}\frac{\partial^3 \phi_y}{\partial y \partial t^2}, \end{aligned} \tag{17a}$$

$$X_{21}\left(w_0\right) + X_{22}\left(\phi_x\right) + X_{23}\left(\phi_y\right) + X_{24}\left(f\right) = \overline{j_2^1}\frac{\partial^2 \phi_x}{\partial t^2} + \overline{j_2^2}\frac{\partial^3 w_0}{\partial x \partial t^2}, \tag{17b}$$

$$X_{31}\left(w_0\right) + X_{32}\left(\phi_x\right) + X_{33}\left(\phi_y\right) + X_{34}\left(f\right) = \overline{j_3^1}\frac{\partial^2 \phi_y}{\partial t^2} + \overline{j_3^2}\frac{\partial^3 w_0}{\partial y \partial t^2}, \tag{17c}$$

where $X_{ij}\left(i = 1 \text{ to } 3, j = 1 \text{ to } 4\right)$, $\overline{j_k^p}\left(k = 1 \text{ to } 3, p = 1 \text{ to } 4\right)$ are presented in Appendix.

The boundary condition can be shown as follows:

$$\begin{aligned} & w_0 = v_0 = w_{,y} = \phi_y = N_{xy} = 0, N_x = N_{x0} \text{ at } x = 0, a \\ & w_0 = u_0 = w_{,x} = \phi_x = N_{xy} = 0, N_y = N_{y0} \text{ at } y = 0, b \end{aligned} \tag{18}$$

The study assumes a plate with all edges as simply supported (SSSS). Using the Galerkin method, approximate solutions of deflection and rotations satisfying the SSSS boundary conditions is derived. This numerical approach is employed to solve partial differential equations by selecting a suitable set of basic functions and subsequently determining coefficients to represent the solution as a linear combination of these functions. This procedure leads to the transformation of the partial differential equation into a system of algebraic equations [32]:

$$\begin{bmatrix} w_0\left(x, y, t\right) \\ \phi_x\left(x, y, t\right) \\ \phi_y\left(x, y, t\right) \end{bmatrix} = \begin{bmatrix} W\left(t\right)\sin \alpha x \sin \beta y \\ \Phi_x\left(t\right)\cos \alpha x \sin \beta y \\ \Phi_y\left(t\right)\sin \alpha x \cos \beta y \end{bmatrix} \tag{19}$$

in which, $\alpha = m\pi / a$, $\beta = n\pi / b$, and $W(t), \Phi_x(t), \Phi_y(t)$ are time dependent displacement and rotation amplitudes, respectively.

The solution form of the stress function $f(x,y,t)$ can be obtain by satisfying the boundary condition and the geometrical compatibility equation [32]:

$$f(x,y,t) = F_1 \cos 2\alpha x + F_2 \cos 2\beta y + F_3 \sin \alpha x \sin \beta y + \frac{1}{2} N_{xo} y^2 \tag{20}$$

in which,

$$F_1 = \frac{1}{32}\frac{\beta^2}{\alpha^2 A_{11}^*} W(t)^2, F_2 = \frac{1}{32}\frac{\alpha^2}{\beta^2 A_{11}^*} W(t)^2, F_3 = \frac{F_{31}}{F_{34}} W(t) + \frac{F_{32}}{F_{34}} \Phi_x(t) + \frac{F_{33}}{F_{34}} \Phi_y(t),$$
$$F_{31} = \left(\alpha^3 c_1 D_{11}^* - \alpha\beta^2 c_1 D_{21}^* + \alpha\beta^2 c_1 D_{66}^* - \alpha^3 B_{11}^* + \alpha\beta^2 B_{21}^* - \alpha\beta^2 B_{66}^*\right),$$
$$F_{32} = \left(\alpha^2 \beta c_1 D_{12}^* - \beta^3 c_1 D_{22}^* + \alpha^2\beta c_1 D_{66}^* - \alpha^2\beta B_{12}^* + \beta^3 B_{22}^* - \alpha^2\beta B_{66}^*\right),$$
$$F_{33} = c_1\left(D_{11}^*\alpha^4 + \alpha^2\beta^2 D_{12}^* - \alpha^2\beta^2 D_{21}^* - D_{22}^*\beta^4 + 2\alpha^2\beta^2 D_{66}^*\right),$$
$$F_{34} = \left(A_{11}^*\alpha^4 - 2A_{12}^*\alpha^2\beta^2 + A_{22}^*\beta^4 + A_{66}^*\alpha^2\beta^2\right).$$

4. Buckling and Free Vibration Analysis

Substituting the solutions from equations (19) and (20) into equations (15) to obtain the resulting equations, and then applying the Galerkin method, we obtain:

$$\begin{aligned}&\left(Y_1^1 + N_{x0}Y_1^8\right)W(t) + Y_1^2 W(t)^2 + Y_1^3 W(t)^3 + Y_1^4\Phi_x(t) + Y_1^5\Phi_y(t) + Y_1^6\Phi_x(t)W(t)\\&+Y_1^7\Phi_y(t)W(t) = I_0\frac{\partial^2 W(t)}{\partial t^2} + \overline{j_1^1}\left(\alpha^2+\beta^2\right)\frac{\partial^2 W(t)}{\partial t^2} - \overline{j_1^3}\alpha\frac{\partial^2\Phi_x(t)}{\partial t^2} - \overline{j_1^4}\beta\frac{\partial^2\Phi_y(t)}{\partial t^2},\end{aligned} \tag{21a}$$

$$Y_2^1 W(t) + Y_2^2 W(t)^2 + Y_2^3\Phi_x(t) + Y_2^4\Phi_y(t) = \overline{j_2^1}\frac{\partial^2\Phi_x(t)}{\partial t^2} + \overline{j_2^2}\alpha\frac{\partial^2 W(t)}{\partial t^2} \tag{21b}$$

$$Y_3^1 W(t) + Y_3^2 W(t)^2 + Y_3^3\Phi_x(t) + Y_3^4\Phi_y(t) = \overline{j_3^1}\frac{\partial^2\Phi_y(t)}{\partial t^2} + \overline{j_3^2}\beta\frac{\partial^2 W(t)}{\partial t^2} \tag{21c}$$

where, $Y_i^j\left(i = 1\text{to}3, j = 1\text{to}8\right)$ can be found in the Appendix.

4.1. Buckling Analysis

In this section, we will discuss the results of the buckling load parameter of the composite plates reinforced by aligned CNTs. The buckling load can be obtained from Eqs. (21) without considering inertial forces and the plates under axial compression with $N_{x0} = -F_x h$:

$$\left(Y_1^1 + N_{x0}Y_1^8\right)W + Y_1^2W^2 + Y_1^3W^3 + Y_1^4\Phi_x + Y_1^5\Phi_y + Y_1^6\Phi_x W + Y_1^7\Phi_y W = 0 \tag{22a}$$

$$Y_2^1 W + Y_2^2 W^2 + Y_2^3\Phi_x + Y_2^4\Phi_y = 0 \tag{22b}$$

$$Y_3^1 W + Y_3^2 W^2 + Y_3^3\Phi_x + Y_3^4\Phi_y = 0 \tag{22c}$$

Upon solving Eqs. (22b) and (22c) to derive Φ_x, Φ_y, and subsequently incorporating them into Eq. (22a), the resulting equation for buckling analysis presents the following form:

$$F_x = L_1 + L_2\bar{W} + L_3\bar{W}^2 \tag{23}$$

where $\bar{W} = \dfrac{W}{h}$, $L_1 = \dfrac{Y_1^1}{Y_1^8 h} + \dfrac{Y_1^5\left(Y_2^1Y_3^3 - Y_2^3Y_3^1\right) - Y_1^4\left(Y_2^1Y_3^4 - Y_2^4Y_3^1\right)}{Y_1^8\left(Y_2^3Y_3^4 - Y_2^4Y_3^3\right)h}$,

$$L_2 = \frac{Y_2^1}{Y_1^8} + \frac{Y_1^5\left(Y_2^2Y_3^3 - Y_2^3Y_3^2\right) - Y_1^4\left(Y_2^2Y_3^4 - Y_2^4Y_3^2\right) - Y_1^6\left(Y_2^1Y_3^4 - Y_2^4Y_3^1\right) + Y_1^7\left(Y_2^1Y_3^3 - Y_2^3Y_3^1\right)}{Y_1^8\left(Y_2^3Y_3^4 - Y_2^4Y_3^3\right)},$$

$$L_3 = \frac{Y_1^3 h}{Y_1^8} + \frac{Y_1^7\left(Y_2^2Y_3^3 - Y_2^3Y_3^2\right)h - Y_1^6\left(Y_2^2Y_3^4 - Y_2^4Y_3^2\right)h}{Y_1^8\left(Y_2^3Y_3^4 - Y_2^4Y_3^3\right)}.$$

The buckling load can be achieved by solving the Eq. (24), in which the lowest value (F_{cr}) is the critical buckling load.

4.2. Free Vibration Analysis

The free vibration of the composite plates reinforced by CNTs can be determined using Eqs. (21) under no external loading ($N_{x0} = 0$). These equations can be rewritten as follows:

$$\begin{aligned}&O_1^1W(t) + O_1^2W(t)^2 + O_1^3W(t)^3 + O_1^4\Phi_x(t) + O_1^5\Phi_y(t) + O_1^6\Phi_x(t)W(t)\\&+O_1^7\Phi_y(t)W(t) = I_0\frac{\partial^2W(t)}{\partial t^2} + \overline{j_1^1}\left(\alpha^2+\beta^2\right)\frac{\partial^2W(t)}{\partial t^2} - \overline{j_1^3}\alpha\frac{\partial^2\Phi_x(t)}{\partial t^2} - \overline{j_1^4}\beta\frac{\partial^2\Phi_y(t)}{\partial t^2},\end{aligned} \tag{24a}$$

$$O_2^1W(t) + O_2^2W(t)^2 + O_2^3\Phi_x(t) + O_2^4\Phi_y(t) = \overline{j_2^1}\frac{\partial^2\Phi_x(t)}{\partial t^2} + \overline{j_2^2}\alpha\frac{\partial^2W(t)}{\partial t^2} \tag{24b}$$

$$O_3^1W(t) + O_3^2W(t)^2 + O_3^3\Phi_x(t) + O_3^4\Phi_y(t) = \overline{j_3^1}\frac{\partial^2\Phi_y(t)}{\partial t^2} + \overline{j_3^2}\beta\frac{\partial^2W(t)}{\partial t^2} \tag{24c}$$

The natural frequencies can be obtained by solving the Eqs. (24) as eigenvalues, in which the lowest value (ω_0) represents the fundamental frequency:

$$\begin{vmatrix} O_1^1 + \omega^2\left(I_0 + \overline{j_1^1}\left(\alpha^2+\beta^2\right)\right) & O_1^4 - \omega^2\overline{j_1^3}\alpha & O_1^5 - \omega^2\overline{j_1^4}\beta \\ O_2^1 + \omega^2\overline{j_2^1}\alpha & O_2^3 + \omega^2\overline{j_2^2} & O_2^4 \\ O_3^1 + \omega^2\overline{j_3^2}\beta & O_3^3 & O_3^4 + \omega^2\overline{j_3^1} \end{vmatrix} = 0 \tag{25}$$

5. Results and Discussion

Mechanical properties of SWCNT (10,10) reinforced polymer matrices are shown in Table 2 [5, 6].

Table 2. The material properties of CNTs and matrix

Materials	Moduli
SWCNT (10,10)	$E_{11}^{CNT} = 5.6466TPa$, $E_{22}^{CNT} = 7.08TPa$, $G_{12}^{CNT} = 1.9445TPa$, $\upsilon_{12}^{CNT} = 0.175$, $\rho^{CNT} = 1400\left(kg/m^3\right)$
PMMA	$E_m = 2.5GPa$, $\upsilon_m = 0.34$, $\rho_m = 1150\left(kg/m^3\right)$
PmPV	$E_m = 2.1GPa$, $\upsilon_m = 0.34$, $\rho_m = 1150\left(kg/m^3\right)$

5.1. Validation

This section presents the outcomes of method verification in this study concerning buckling load and fundamental frequency parameters for composite plates reinforced with CNTs. Table 3 provides a comparison of the buckling load parameter $\bar{N} = \frac{F_{cr} b^2}{E_m h^3}$ for PmPV plates reinforced with CNTs under axial loading with $b/h = 10, a = b = 1$. Tables 4 and 5 compare the dimensionless fundamental frequency $\varpi = \omega_0 \frac{b^2}{h}\sqrt{\frac{\rho_m}{E_m}}$ of composite plates reinforced with CNTs using PmPV and PMMA matrices, respectively ($h/a = 0.1, b = a$)

Table 3. Comparison of dimensionless buckling parameter of CNTs reinforced composite plates

CNT volume fraction	UD		FG-X	
	Ref. [20]	Present	Ref. [20]	Present
$V_{CNT}^* = 0.11$	13.9658	13.3377	16.5819	15.4660
$V_{CNT}^* = 0.14$	14.8509	14.9671	18.1138	17.0176
$V_{CNT}^* = 0.17$	22.0602	20.8645	24.5714	24.0020

Table 4. Dimensionless fundamental frequency of PmPV plates reinforced by CNTs

CNT volume fraction	Types of CNTs	Ref. [21]	Ref. [22]	Present
$V_{CNT}^* = 0.11$	UD	13.532	13.735	12.9991
	FG-X	14.616	14.873	13.9990
	FG-O	11.550	11.675	10.9706
$V_{CNT}^* = 0.14$	UD	14.306	14.553	13.7271
	FG-X	12.338	15.669	14.6384
	FG-O	15.368	12.501	11.7092
$V_{CNT}^* = 0.17$	UD	16.815	16.832	16.0859
	FG-X	18.278	18.377	17.3294
	FG-O	14.282	14.563	13.6543

Table 5. Comparison study of dimensionless fundamental frequency of CNTs reinforced PMMA plates

	CNT volume fraction	$a/h=10$		$a/h=50$	
		Ref. [23]	Present	Ref. [23]	Present
UD	$V_{CNT}^*=0.12$	14.181	12.8741	17.808	17.7120
	$V_{CNT}^*=0.17$	17.562	16.0939	21.536	21.4436
	$V_{CNT}^*=0.28$	20.343	19.8906	26.620	26.4271
FG-X	$V_{CNT}^*=0.12$	15.734	13.9816	21.343	21.1589
	$V_{CNT}^*=0.17$	17.656	17.5191	25.858	25.6591
	$V_{CNT}^*=0.28$	22.798	21.1687	32.167	31.6993
FG-O	$V_{CNT}^*=0.12$	11.576	10.7641	13.264	13.2235
	$V_{CNT}^*=0.17$	14.202	13.3857	16.014	15.9818
	$V_{CNT}^*=0.28$	16.737	15.6145	19.515	19.4582

5.2. Buckling Analysis

Tables 6 and 7 present the influence of CNT distribution and volume fraction on the buckling load parameter of composite plates subjected to axial loading, using PMMA and PmPV matrices. Furthermore, Figure 3 illustrates the mode shapes of composite plates reinforced by aligned CNTs.

Three different CNT volume fractions are investigated $V_{CNT}^*=\left(0.12, 0.17, 0.28\right)$ for PMMA plates reinforced by CNTs and $V_{CNT}^*=\left(0.11, 0.14, 0.17\right)$ for PmPV plates reinforced by CNTs. Gernally, for both matrices, the buckling load parameter ($\bar{N}=\dfrac{F_{cr}b^2}{E_m h^3}$) increases as CNT volume fraction increases. This can be explained by the rise in the volume fraction of CNTs, which leads to higher strength and an elevated buckling load. This effect is due to the significantly greater stiffness of CNTs compared to that of the polymer matrix.

Table 6. Dimensionless buckling parameter of CNTs reinforced PMMA plates

CNT's volume fraction	UD	FG-X	FG-O
$V_{CNT}^*=0.12$	13.2255	15.5962	9.2478
$V_{CNT}^*=0.17$	20.8882	24.7471	14.4533
$V_{CNT}^*=0.28$	27.4156	31.0455	20.1192

Table 7. Dimensionless buckling parameter of CNTs reinforced PmPV plates

CNT's volume fraction	UD	FG-X	FG-O
$V_{CNT}^*=0.11$	13.3377	15.4660	9.5023
$V_{CNT}^*=0.14$	14.9671	17.0176	10.8930
$V_{CNT}^*=0.17$	20.8645	24.0020	14.9077

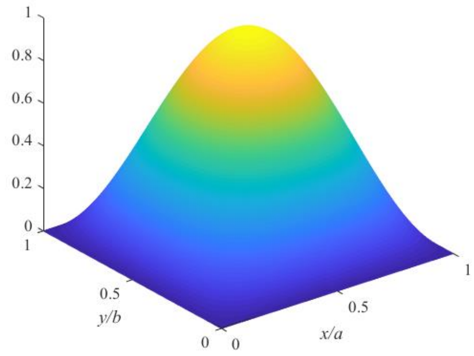

a. Mode 1 ($m = n = 1$)

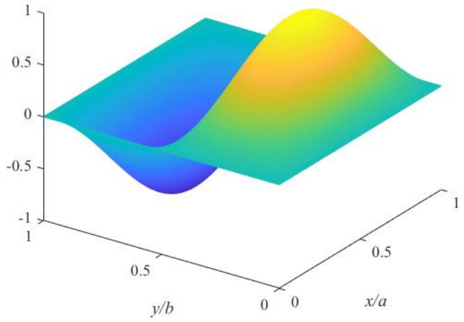

b. Mode 2 ($m = 1, n = 1$)

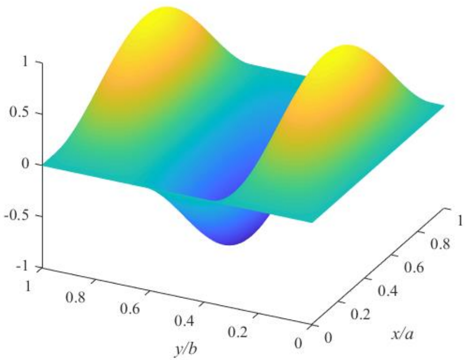

c. Mode 3 ($m = 1, n = 3$)

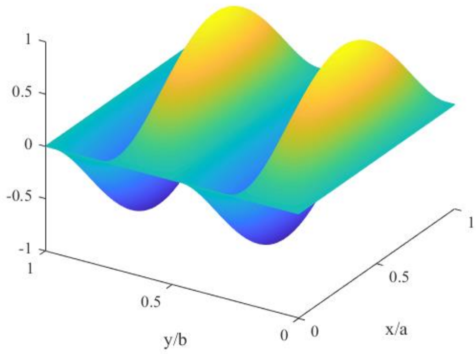

d. Mode 4 ($m = 1, n = 4$)

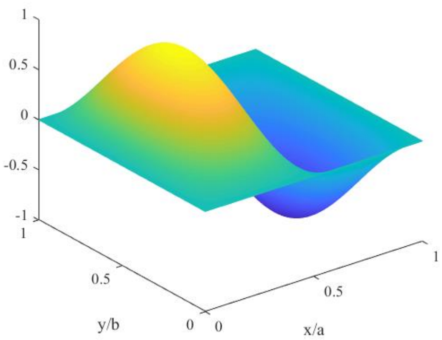

e. Mode 5 ($m = 2, n = 1$)

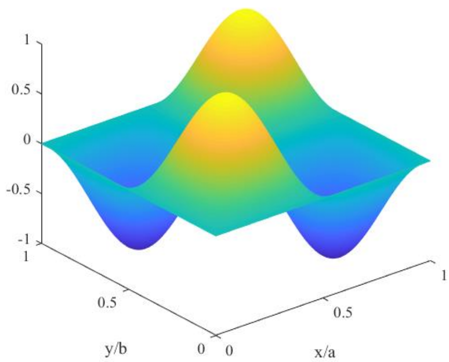

f. Mode 6 ($m = n = 2$)

Figure 3. Mode shapes of CNTs reinforced composite plates.

5.3. Free Vibration Analysis

Table 8 illustrates the effect of the aspect ratio on the dimensionless fundamental frequency of polymer plates reinforced with UD CNTs, using PMMA and PmPV matrices. The figures demonstrate a decrease in the fundamental frequency parameter as the a/b ratio increases. It becomes evident that when all other geometric parameters remain constant, an increase in the a/b ratio leads to a higher plate aspect ratio resulting in reduced strength.

Table 8. The effect of a/b ratio on the dimensionless fundamental frequency of composite plates reinforced by UD-CNTs (h/b=0.1)

a/b	PMMA			PmPV		
	$V_{CNT}^{*}=0.12$	$V_{CNT}^{*}=0.17$	$V_{CNT}^{*}=0.28$	$V_{CNT}^{*}=0.11$	$V_{CNT}^{*}=0.14$	$V_{CNT}^{*}=0.17$
1	12.8741	16.0939	19.8906	12.9991	13.7271	16.0859
1.5	7.3681	9.1737	10.5134	7.4839	7.9788	9.2857
2	5.1757	6.4813	7.3359	5.2192	5.5503	6.4790
2.5	4.1855	5.2872	5.8607	4.1604	4.3845	5.1728
3	3.6984	4.7066	5.1216	3.6267	3.7849	4.5169

Table 9. The effect of b/h ratios on the dimensionless fundamental frequency of PMMA plates reinforced by CNTs (a/b=1)

b/h ratio	CNT volume fraction	UD	FG-X	FG-O
b/h=10	$V_{CNT}^{*}=0.12$	12.8741	13.9816	10.7641
	$V_{CNT}^{*}=0.17$	16.0939	17.5191	13.3857
	$V_{CNT}^{*}=0.28$	19.8906	21.1687	15.6145
b/h=20	$V_{CNT}^{*}=0.12$	16.1590	18.6119	12.5275
	$V_{CNT}^{*}=0.17$	19.7857	22.8644	15.2715
	$V_{CNT}^{*}=0.28$	23.6435	26.9620	18.3558
b/h=30	$V_{CNT}^{*}=0.12$	17.1338	20.1769	12.9738
	$V_{CNT}^{*}=0.17$	20.8332	24.5946	15.7292
	$V_{CNT}^{*}=0.28$	25.3710	29.8120	19.0613
b/h=50	$V_{CNT}^{*}=0.12$	17.7120	21.1589	13.2235
	$V_{CNT}^{*}=0.17$	21.4436	25.6591	15.9818
	$V_{CNT}^{*}=0.28$	26.4271	31.6993	19.4582

Table 9 and Figure 4 illustrate the impact of CNT distribution and width-to-thickness ratio on the fundamental frequency parameter of CNT reinforced composite plates with PMMA and PmPV matrices, respectively. An important observation is that the fundamental frequency parameter in the case of FG-X distribution is higher than the that in the case of UD and FG-O distributions. This phenomenon arises due to the variation in CNT volume fraction along the plate's mid-plane region. FG-X exhibits the highest CNT volume fraction in this area, where stress tends to approach zero, while FG-O shows the lowest CNT volume fraction. As a result, in the case of FG-O, the increased CNT volume fraction in this region remains underutilized since stress levels are negligible. Consequently, the plate's strength is lower in the FG-O case, resulting in a reduced fundamental frequency and buckling load parameter compared to the FG-X distribution.

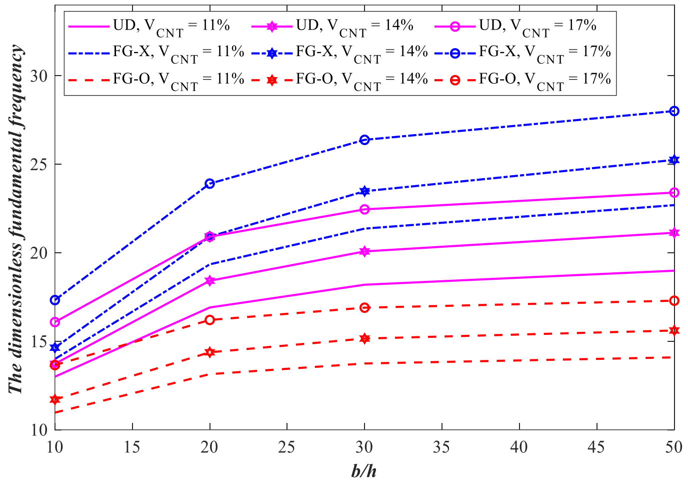

Figure 4. Effect of CNT's distribution and volume fraction on the fundamental frequency parameter of PmPV plates (a/b=1).

6. Conclusion

In this work, we investigated the buckling and free vibration behavior of polymer plates reinforced with aligned carbon nanotubes. We utilized an analytical approach using the third-order shear deformation plate theory, incorporating von Kármán's geometric nonlinearity to derive the governing equations. Furthermore, we conducted an extensive parametric analysis to assess the influence of factors such as CNT's distribution, CNT's volume fraction, and geometric parameters on the buckling and fundamental frequency parameters of the plates. The results of this investigation are summarized as follows:

- Elevated CNT volume fractions enhance the strength of composite plates, as well as increasing buckling load and fundamental frequency parameters.

- The buckling load and fundamental frequency parameters of the composite plates increase as the volume fraction of CNTs increases from the middle layer to the outer layer of the plates. The strength of polymer plates is highest when reinforced with FG-X CNTs and lowest in the case of FG-O distribution.

- The effect of geometric parameters on buckling and free vibration analysis of CNTs reinforced composite plates is discussed. It is observed that the strength of the plates decreases when aspect ratio (*a/b*) is increased.

Acknowledgements

This research is funded by the Project number CN.22.11 of VNU Hanoi – University of Engineering and Technology. The authors are grateful for this support.

Appendix

$$X_{11}(w_0) = f_{10}\frac{\partial^4 w_0}{\partial x^2 \partial y^2} + f_{11}\frac{\partial^4 w_0}{\partial x^4} + f_{12}\frac{\partial^4 w_0}{\partial y^4} - f_{13}\frac{\partial^2 w_0}{\partial x^2} + f_{14}\frac{\partial^2 w_0}{\partial y^2} - K_w w_0 + K_p \nabla^2 w_0,$$

$$X_{12}\left(\phi_x\right) = f_4\frac{\partial \varphi_x}{\partial x} + f_5\frac{\partial^3 \varphi_x}{\partial x^3} + f_6\frac{\partial^3 \varphi_x}{\partial x \partial y^2}, X_{13}\left(\phi_y\right) = f_7\frac{\partial \varphi_y}{\partial y} + f_8\frac{\partial^3 \varphi_y}{\partial y^3} + f_9\frac{\partial^3 \varphi_y}{\partial x^2 \partial y},$$

$$X_{14}\left(f\right) = f_1\frac{\partial^4 f}{\partial x^2 \partial y^2} + f_2\frac{\partial^4 f}{\partial x^4} + f_3\frac{\partial^4 f}{\partial y^4}, X_{15}\left(w_0, f\right) = \frac{\partial^2 f}{\partial y^2}\frac{\partial^2 w_0}{\partial x^2} - 2\frac{\partial^2 f}{\partial x \partial y}\frac{\partial^2 w_0}{\partial x \partial y} + \frac{\partial^2 f}{\partial x^2}\frac{\partial^2 w_0}{\partial y^2},$$

$$X_{21}\left(w_0\right) = m_6\frac{\partial^3 w_0}{\partial x \partial y^2} + m_7\frac{\partial^3 w_0}{\partial x^3} + m_9\frac{\partial w_0}{\partial x}, X_{22}\left(\phi_x\right) = m_3\frac{\partial^2 \phi_x}{\partial x^2} + m_4\frac{\partial^2 \phi_x}{\partial y^2} + m_8\phi_x,$$

$$X_{23}\left(\phi_y\right) = m_5\frac{\partial^2 \phi_y}{\partial x \partial y}, X_{24}(f) = m_1\frac{\partial^3 f}{\partial x^3} + m_2\frac{\partial^3 f}{\partial x \partial y^2}, X_{31}\left(w_0\right) = l_6\frac{\partial^3 w_0}{\partial x^2 \partial y} + l_7\frac{\partial^3 w_0}{\partial y^3} + l_9\frac{\partial w_0}{\partial y},$$

$$X_{32}\left(\phi_x\right) = l_3\frac{\partial^2 \phi_x}{\partial x \partial y}, X_{33}\left(\phi_y\right) = l_4\frac{\partial^2 \phi_y}{\partial x^2} + l_5\frac{\partial^2 \phi_y}{\partial y^2} + l_8\phi_y,\ X_{34}(f) = l_1\frac{\partial^3 f}{\partial x^2 \partial y} + l_2\frac{\partial^3 f}{\partial y^3},$$

$$\overline{j_1^1} = \overline{j_1^2} = \left(\frac{c_1^2 I_3^2}{I_0} - c_1^2 I_6\right), \overline{j_1^3} = \overline{j_1^4} = c_1\left(J_4 - \frac{J_1 I_3}{I_0}\right),$$

$$\overline{j_2^1} = \left(K_2 - \frac{J_1^2}{I_0}\right), \overline{j_2^2} = \left(\frac{c_1 I_3 J_1}{I_0} - c_1 J_4\right), \overline{j_3^1} = \left(K_2 - \frac{J_1^2}{I_0}\right), \overline{j_3^2}\left(\frac{c_1 I_3 J_1}{I_0} - c_1 J_4\right).$$

$$f_1 = \left(c_1 D_{11} A_{22}^* - c_1 D_{12} A_{12}^* + c_1 D_{22} A_{11}^* - c_1 D_{12} A_{21}^* - 2c_1 D_{66} A_{66}^*\right), f_2 = \left(c_1 D_{12} A_{11}^* - c_1 D_{11} A_{21}^*\right),$$

$$f_3 = \left(c_1 D_{12} A_{22}^* - c_1 D_{22} A_{12}^*\right), f_4 = \left(-3c_1 C_{44} + 3c_1 c_2 E_{44} + A_{44} - c_2 C_{44}\right),$$

$$f_5 = \left(c_1 D_{12} B_{11}^* - c_1 D_{11} B_{21}^* + c_1 E_{11} - c_1^2 D_{12} D_{11}^* + c_1^2 D_{11} D_{21}^* - c_1^2 G_{11}\right),$$

$$f_6 = 2c_1^2\left(D_{66} D_{66}^* - G_{66}\right) + c_1\left(D_{22} B_{11}^* - D_{12} B_{21}^* + E_{12}\right) + c_1^2\left(D_{12} D_{21}^* - G_{12} - D_{22} D_{11}^*\right) + 2c_1\left(E_{66} - D_{66} B_{66}^*\right),$$

$$f_7 = \left(-3c_1 C_{55} + 3c_1 c_2 E_{55} + A_{55} - c_2 C_{55}\right),$$

$$f_8 = \left(c_1 D_{22} B_{12}^* - c_1 D_{12} B_{22}^* + c_1 E_{22} - c_1^2 D_{22} D_{12}^* + c_1^2 D_{12} D_{22}^* - c_1^2 G_{22}\right),$$

$$f_9 = \begin{pmatrix} c_1 D_{12} B_{12}^* - c_1 D_{11} B_{22}^* + c_1 E_{12} - c_1^2 D_{12} D_{12}^* + c_1^2 D_{11} D_{22}^* - c_1^2 G_{12} \\ +2c_1 E_{66} - 2c_1 D_{66} B_{66}^* - 2c_1^2 G_{66} + 2c_1^2 D_{66} D_{66}^* \end{pmatrix},$$

$$f_{10} = \left(-c_1^2 D_{12} D_{12}^* + c_1^2 D_{11} D_{22}^* - c_1^2 G_{12} - 4c_1^2 G_{66} + 4c_1^2 D_{66} D_{66}^* - c_1^2 D_{22} D_{11}^* + c_1^2 D_{12} D_{21}^* - c_1^2 G_{12}\right),$$

$$f_{11} = \left(-c_1^2 D_{12} D_{11}^* + c_1^2 D_{11} D_{21}^* - c_1^2 G_{11}\right), f_{12} = \left(-c_1^2 D_{22} D_{12}^* + c_1^2 D_{12} D_{22}^* - c_1^2 G_{22}\right),$$

$$f_{13} = \left(A_{44} - c_2 C_{44} - 3c_1 C_{44} + 3c_1 c_2 E_{44}\right), f_{14} = \left(A_{55} - c_2 C_{55} - 3c_1 C_{55} + 3c_1 c_2 E_{55}\right).$$

$$m_1 = \left(B_{12} A_{11}^* - B_{11} A_{21}^* - c_1 D_{12} A_{11}^* + c_1 D_{11} A_{21}^*\right),$$

$$m_2 = \left(B_{11} A_{22}^* - B_{12} A_{12}^* - B_{66} A_{66}^* - c_1 D_{11} A_{22}^* + c_1 D_{12} A_{12}^* + c_1 D_{66} A_{66}^*\right),$$

$$m_3 = \begin{pmatrix} B_{12} B_{11}^* - B_{11} B_{21}^* + C_{11} - c_1 D_{12} B_{11}^* + c_1 D_{11} B_{21}^* - c_1 E_{11} - \\ c_1 B_{12} D_{11}^* + c_1 B_{11} D_{21}^* - c_1 E_{11} + c_1^2 D_{12} D_{11}^* - c_1^2 D_{11} D_{21}^* + c_1^2 G_{11} \end{pmatrix},$$

$$m_4 = \left(-c_1 E_{66} + c_1 B_{66} D_{66}^* + c_1^2 G_{66} - c_1^2 D_{66} D_{66}^* + C_{66} - B_{66} B_{66}^* - c_1 E_{66} + c_1 D_{66} B_{66}^*\right),$$

$$m_5 = \begin{pmatrix} C_{66} - B_{66}B_{66}^* - c_1E_{66} + c_1D_{66}B_{66}^* - c_1E_{66} + c_1B_{66}D_{66}^* + c_1^2G_{66} - c_1^2D_{66}D_{66}^* \\ +B_{12}B_{12}^* - B_{11}B_{22}^* + C_{12} - c_1D_{12}B_{12}^* + c_1D_{11}B_{22}^* - c_1E_{12} - c_1B_{12}D_{12}^* \\ +c_1B_{11}D_{22}^* - c_1E_{12} + c_1^2D_{12}D_{12}^* - c_1^2D_{11}D_{22}^* + c_1^2G_{12} \end{pmatrix},$$

$$m_6 = \begin{pmatrix} -2c_1E_{66} + 2c_1B_{66}D_{66}^* + 2c_1^2G_{66} - 2c_1^2D_{66}D_{66}^* - c_1B_{12}D_{12}^* + c_1B_{11}D_{22}^* \\ -c_1E_{12} + c_1^2D_{12}D_{12}^* - c_1^2D_{11}D_{22}^* + c_1^2G_{12} \end{pmatrix},$$

$$m_7 = \left(-c_1B_{12}D_{11}^* + c_1B_{11}D_{21}^* - c_1E_{11} + c_1^2D_{12}D_{11}^* - c_1^2D_{11}D_{21}^* + c_1^2G_{11}\right),$$
$$m_8 = c_2C_{44} - A_{44} + 3c_1\left(C_{44} - c_2E_{44}\right), m_9 = c_2C_{44} - A_{44} + 3c_1\left(C_{44} - c_2E_{44}\right),$$

$$l_1 = \left(B_{22}A_{11}^* - B_{12}A_{21}^* - B_{66}A_{66}^* - c_1D_{22}A_{11}^* + c_1D_{12}A_{21}^* + c_1D_{66}A_{66}^*\right),$$
$$l_2 = \left(B_{12}A_{22}^* - B_{22}A_{12}^* - c_1D_{12}A_{22}^* + c_1D_{22}A_{12}^*\right),$$
$$l_3 = \begin{pmatrix} C_{66} - B_{66}B_{66}^* - c_1E_{66} + c_1D_{66}B_{66}^* + B_{22}B_{11}^* - B_{12}B_{21}^* + C_{12} - c_1D_{22}B_{11}^* \\ +c_1D_{12}B_{21}^* - c_1E_{12} - c_1B_{22}D_{11}^* + c_1B_{12}D_{21}^* - c_1E_{12} + c_1^2D_{22}D_{11}^* \\ -c_1^2D_{12}D_{21}^* + c_1^2G_{12} - c_1E_{66} + c_1B_{66}D_{66}^* + c_1^2G_{66} - c_1^2D_{66}D_{66}^* \end{pmatrix},$$

$$l_4 = \left(C_{66} - B_{66}B_{66}^* - c_1E_{66} + c_1D_{66}B_{66}^* - c_1E_{66} + c_1B_{66}D_{66}^* + c_1^2G_{66} - c_1^2D_{66}D_{66}^*\right),$$
$$l_5 = \begin{pmatrix} B_{22}B_{12}^* - B_{12}B_{22}^* + C_{22} - c_1D_{22}B_{12}^* + c_1D_{12}B_{22}^* - c_1E_{22} - c_1B_{22}D_{12}^* \\ +c_1B_{12}D_{22}^* - c_1E_{22} + c_1^2D_{22}D_{12}^* - c_1^2D_{12}D_{22}^* + c_1^2G_{22} \end{pmatrix},$$

$$l_6 = \begin{pmatrix} -2c_1E_{66} + 2c_1B_{66}D_{66}^* + 2c_1^2G_{66} - 2c_1^2D_{66}D_{66}^* - c_1B_{22}D_{11}^* + c_1B_{12}D_{21}^* \\ -c_1E_{12} + c_1^2D_{22}D_{11}^* - c_1^2D_{12}D_{21}^* + c_1^2G_{12} \end{pmatrix},$$
$$l_7 = c_1\left(D_{22}^*B_{12} - B_{22}D_{12}^* - E_{22}\right) + c_1^2\left(D_{22}D_{12}^* - D_{12}D_{22}^* + G_{22}\right),$$
$$l_8 = c_2C_{55} - A_{55} + 3c_1\left(C_{55} - c_2E_{55}\right), l_9 = c_2C_{55} - A_{55} - 3c_1\left(c_2E_{55} + C_{55}\right).$$

$$Y_1^1 = f_1\frac{F_{33}}{F_{34}}\alpha^2\beta^2 + f_2\frac{F_{33}}{F_{34}}\alpha^4 + f_3\frac{F_{33}}{F_{34}}\beta^4 + f_{10}\alpha^2\beta^2 + f_{11}\alpha^4 + f_{12}\beta^4 - f_{13}\alpha^2 - f_{14}\beta^2 - K_w - K_p\left(\alpha^2 + \beta^2\right),$$

$$Y_1^2 = \frac{8}{3}\frac{\alpha^2\beta^2}{n\pi^2 m}\left(4\frac{F_{33}}{F_{34}} - \left(\frac{f_2}{A_{11}^*} + \frac{f_3}{A_{22}^*}\right)\right), Y_1^3 = -\left(\frac{\alpha^4}{16A_{22}^*} + \frac{\beta^4}{16A_{11}^*}\right),$$

$$Y_1^4 = \left(f_1\frac{F_{31}}{F_{34}}\alpha^2\beta^2 + f_2\frac{F_{31}}{F_{34}}\alpha^4 + f_3\frac{F_{31}}{F_{34}}\beta^4 - f_4\alpha + f_5\alpha^3 + f_6\alpha\beta^2\right),$$
$$Y_1^5 = \left(f_1\frac{F_{32}}{F_{34}}\alpha^2\beta^2 + f_2\frac{F_{32}}{F_{34}}\alpha^4 + f_3\frac{F_{32}}{F_{34}}\beta^4 - f_7\beta + f_8\beta^3 + f_9\beta\alpha^2\right),$$

$$Y_1^6 = \frac{32}{3}\frac{\alpha^2\beta^2}{n\pi^2 m}\frac{F_{31}}{F_{34}}, Y_1^7 = \frac{32}{3}\frac{\alpha^2\beta^2}{n\pi^2 m}\frac{F_{32}}{F_{34}}, Y_1^8 = -\frac{1}{4}ab\alpha^2,$$
$$Y_2^1 = -\left(m_7\alpha^3 + m_6\alpha\beta^2 + m_1\frac{F_{33}}{F_{34}}\alpha^3 + m_2\frac{F_{33}}{F_{34}}\alpha\beta^2 - m_9\alpha\right), Y_2^2 = \frac{8\beta m_1}{3A_{11}^*ab},$$

$$Y_2^3 = -\left(m_1 \frac{F_{31}}{F_{34}} \alpha^3 + m_2 \frac{F_{31}}{F_{34}} \alpha\beta^2 + m_3\alpha^2 + m_4\beta^2 - m_8 \right),$$

$$Y_2^4 = -\left(m_5\alpha\beta + m_1 \frac{F_{32}}{F_{34}} \alpha^3 + m_2 \frac{F_{32}}{F_{34}} \alpha\beta^2 \right),$$

$$Y_3^1 = -\left(l_6\alpha^2\beta + l_7\beta^3 + l_1 \frac{F_{33}}{F_{34}} \alpha^2\beta + l_2 \frac{F_{33}}{F_{34}} \beta^3 - l_9\beta \right), Y_3^2 = \frac{8\alpha l_2}{3A_{22}^* ab},$$

$$Y_3^3 = -\left(\alpha\beta l_3 + l_1 \frac{F_{31}}{F_{34}} \alpha^2\beta + l_2 \frac{F_{31}}{F_{34}} \beta^3 \right), Y_3^4 = -\left(l_4\alpha^2 + l_5\beta^2 - l_8 + l_1 \frac{F_{32}}{F_{34}} \alpha^2\beta + l_2 \frac{F_{32}}{F_{34}} \beta^3 \right),$$

References

[1] C. F. Deng, D. Z. Wang, X. X. Zhang, Y. X. Ma, Damping Characteristics of Carbon Nanotube Reinforced Aluminium Composite, Mater. Lett., Vol. 61, 2007, pp. 3229-3231, https://doi.org/10.1016/j.matlet.2006.11.073.

[2] F. D. Borbón, D. Ambrosini, Dynamic Response of Composites Sandwich Plates with Carbon Nanotubes Subjected to Blast Loading, Compos. B. Eng., Vol. 45, 2013, pp. 466-73, https://doi.org/10.1016/j.compositesb.2012.07.035.

[3] G. J. Wang, Y. P. Cai, Y. J. Ma, S. C. Tang, J. A. Syed, Z. H. Cao, X. K. Meng, Ultrastrong and Stiff Carbon Nanotube/Aluminum-Copper Nanocomposite via Enhancing Friction between Carbon Nanotubes, Nano Lett., Vol. 19, 2019, pp. 6255-62, https://doi.org/10.1021/acs.nanolett.9b02332.

[4] S. Pal, P. N. B. Babu, B. S. K. Gargeya, C. S. Becquart, Molecular Dynamics Simulation-Based Investigation of Possible Enhancement in Strength and Ductility of Nanocrystalline Aluminum by CNT Reinforcement, Mater. Chem. Phys., Vol. 243, 2020, pp. 122593, https://doi.org/10.1016/j.matchemphys.2019.122593.

[5] H. S. Shen, Nonlinear Bending of Functionally Graded Carbon Nanotube-Reinforced Composite Plates in Thermal Environments, Compos. Struct., Vol. 91, 2009, pp. 9-19, https://doi.org/10.1016/j.compstruct.2009.04.026.

[6] H. S. Shen, H. Z. Zheng, Buckling and Postbuckling Behavior of Functionally Graded Nanotube-Reinforced Composite Plates in Thermal Environments, Comput. Mater. Contin, Vol. 18, 2010, pp. 155-182, https://doi.org/10.3970/cmc.2010.018.155.

[7] P. Kumar, J. Srinivas, Vibration, Buckling and Bending Behavior of Functionally Graded Multiwalled Carbon Nanotube Reinforced Polymer Composite Plates using the Layer-Wise Formulation, Compos. Struct., Vol. 177, 2017, pp. 158-170, https://doi.org/10.1016/j.compstruct.2017.06.055.

[8] R. Gholami, R. Ansari, Y. Gholami, Numerical Study on the Nonlinear Resonant Dynamics of Carbon Nanotube/Fiber/Polymer Multiscale Laminated Composite Rectangular Plates with Various Boundary Conditions, Aerosp. Sci. Technol., Vol. 78, 2018, pp. 118-129, https://doi.org/10.1016/j.ast.2018.03.043.

[9] D. L. Shi, X. Q. Feng, Y. Y. Huang, K. C. Hwang, H. J. Gao, The Effect of Nanotube Waviness and Agglomeration on the Elastic Property of Carbon Nanotube-Reinforced Composites, Compos. Struct., Vol. 63, 2004, pp. 305-313, https://doi.org/10.1115/1.1751182.

[10] P. Malekzadeh, M. Dehbozorgi, M. Monajjemzadeh, Vibration of Functionally Graded Carbon Nanotube-Reinforced Composite Plates Under A Moving Load, Sci. Eng. Compos., Vol. 22, 2013, pp. 37-55, https://doi.org/10.1515/secm-2013-0142.

[11] L. W. Zhang, Z. X. Lei, K. M. Liew, Buckling Analysis of FG-CNT Reinforced Composite Thick Skew Plates Using An Element-Free Approach, Compos. Part B: Eng., Vol. 75, 2015, pp. 36-46, https://doi.org/10.1016/j.compositesb.2015.01.033.

[12] L. W. Zhang, K. M. Liew, Postbuckling Analysis of Axially Compressed CNT Reinforced Functionally Graded Composite Plates Resting on Pasternak Foundations using An Element-Free Approach, Compos. Struct., Vol. 138, 2016, pp. 40-51, https://doi.org/10.1016/j.compstruct.2015.11.031.

[13] J. Torabi, R. Ansari, R. Hassani, Numerical Study on the Thermal Buckling Analysis of CNT-Reinforced Composite Plates with Different Shapes Based on the Higher-Order Shear Deformation Theory, Eur. J. Mech. A Solids, Vol. 73, 2019, pp. 144-160, https://doi.org/10.1016/j.euromechsol.2018.07.009.

[14] J. Peng, C. Zhiping, M. He, Z. Delin, G. Peng, Buckling Analysis of Thin Rectangular FG-CNTRC Plate Subjected to Arbitrarily Distributed Partial Edge Compression Loads Based on Differential Quadrature Method, Thin-Walled Struct., Vol. 145, 2019, pp. 106417, https://doi.org/10.1016/j.tws.2019.106417.

[15] O. Civaleka, M. H. Jalaei, Shear Buckling Analysis of Functionally Graded (FG) Carbon Nanotube Reinforced Skew Plates with Different Boundary Conditions, Aerosp. Sci. Technol., Vol. 99, 2020, pp. 105753, https://doi.org/10.1016/j.ast.2020.105753.

[16] M. Mirzaei, Y. Kiani, Thermal Buckling of Temperature Dependent FG-CNT Reinforced Composite Plates, Meccanica., Vol. 47, 2015, pp. 1-17, https://doi.org/10.1007/s11012-015-0348-0.

[17] Y. Kiani, Shear Buckling of FG-CNT Reinforced Composite Plates Using Chebyshev-Ritz Method, Compos Part B: Eng., Vol. 105, 2016, pp. 176-187, https://doi.org/10.1016/j.compositesb.2016.09.001.

[18] Y. Kiani, Thermal Post-Buckling of FG-CNT Reinforced Composite Plates, Compos. Struct., Vol. 159, 2017, pp. 299-306, https://doi.org/10.1016/j.compstruct.2016.09.084.

[19] Y. Kiani, M. Mirzaei, Rectangular and Skew Shear Buckling of FG-CNT Reinforced Composite Skew Plates using Ritz Method, Aerosp. Sci. Technol., Vol. 77, 2018, pp. 388-398, https://doi.org/10.1016/j.ast.2018.03.022.

[20] A. Hussain, Buckling Analysis of Functionally Graded Carbon Nanotubes Reinforced Composite (Fg-Cntrc) Plate. Thesis, National Institute of Technology Rourkela, India, 2014.

[21] P. P. Van, M. A. Wahab, K. M. Liew, S. P. A. Bordas, H. N. Xuan, Isogeometric Analysis of Functionally Graded Carbon Nanotube-Reinforced Compositeoflates using Higher-Order Shear Deformation Theory, Compos. Struct., Vol. 123, 2015, pp. 137-149, https://doi.org/10.1016/j.compstruct.2014.12.021.

[22] A. K. Singh, A. Bhar, Isogeometric FE Analysis of CNT-Reinforced Composite Plates: Free Vibration, SN Applied Sciences, Vol. 1, 2019, pp. 1010, https://doi.org/10.1007/s42452-019-1027-x.

[23] E. G. Macías, R. C. Triguero, E. I. S. Flores, M. I. Friswell, R. Gallego, Static and Free Vibration Analysis of Functionally Graded Carbon Nanotube Reinforced Skew Plates, Compos. Struct., Vol. 140, 2016, pp. 473-490, https://doi.org/10.1016/j.compstruct.2015.12.044.

[24] Z. X. Lei, K. M. Liew, J. L. Yu, Free Vibration Analysis of Functionally Graded Carbon Nanotube-Reinforced Composite Plates using the Element-Free Kp-Ritz Method in Thermal Environment, Compos. Struct., Vol. 106, 2013, pp. 128-138, https://doi.org/10.1016/j.compstruct.2013.06.003.

[25] L. W. Zhang, W. C. Cui, K. M. Liew, Vibration Analysis of Functionally Graded Carbon Nanotube Reinforced Composite Thick Plates with Elastically Restrained Edges, Int. J. Mech. Sci., Vol. 103, 2015, pp. 9-21, https://doi.org/10.1016/j.ijmecsci.2015.08.021.

[26] L.W. Zhang, Z. X. Lei, K. M. Liew, Free Vibration Analysis of Functionally Graded Carbon Nanotube-Reinforced Composite Triangular Plates using the FSDT and Element-Free Imls-Ritz Method, Compos. Struct., Vol. 120, 2015, pp. 189-199, https://doi.org/10.1016/j.compstruct.2014.10.009.

[27] N. Fantuzzi, F. Tornabene, M. Bacciocchi, R. Dimitri, Free Vibration Analysis of Arbitrarily Shaped Functionally Graded Carbon Nanotube-Reinforced Plates, Compos. Part B: Eng., Vol. 115, 2017, pp. 384-408, https://doi.org/10.1016/j.compositesb.2016.09.021.

[28] E. G. Macías, R. C. Triguero, M. I. Friswell, S. Adhikari, A. Sáez, Metamodel-Based Approach for Stochastic Free Vibration Analysis of Functionally Graded Carbon Nanotube Reinforced Plates, Compos. Struct., Vol. 152, 2016, pp. 183-198, https://doi.org/10.1016/j.compstruct.2016.05.019.

[29] E. G. Macías, L. R. Tembleque, A. Sáez, Bending and Free Vibration Analysis of Functionally Graded Graphene vs Carbon Nanotube Reinforced Composite Plates, Compos. Struct., Vol. 186, 2018, pp. 123-138, https://doi.org/10.1016/j.compstruct.2017.11.076.

[30] A. Karamanli, M. Aydogdu, Vibration Behaviors of Two-Directional Carbon Nanotube Reinforced Functionally Graded Composite Plates, Compos. Struct., Vol. 262, 2021, pp. 113639, https://doi.org/10.1016/j.compstruct.2021.113639.

[31] J. N. Reddy, Mechanics of Laminated Composite Plates and Shells, CRC Press, 2004.

[32] N. D. Duc, Nonlinear Static and Dynamic Stability of Functionally Graded Plates and Shells, Vietnam National University Press, Hanoi, 2014.